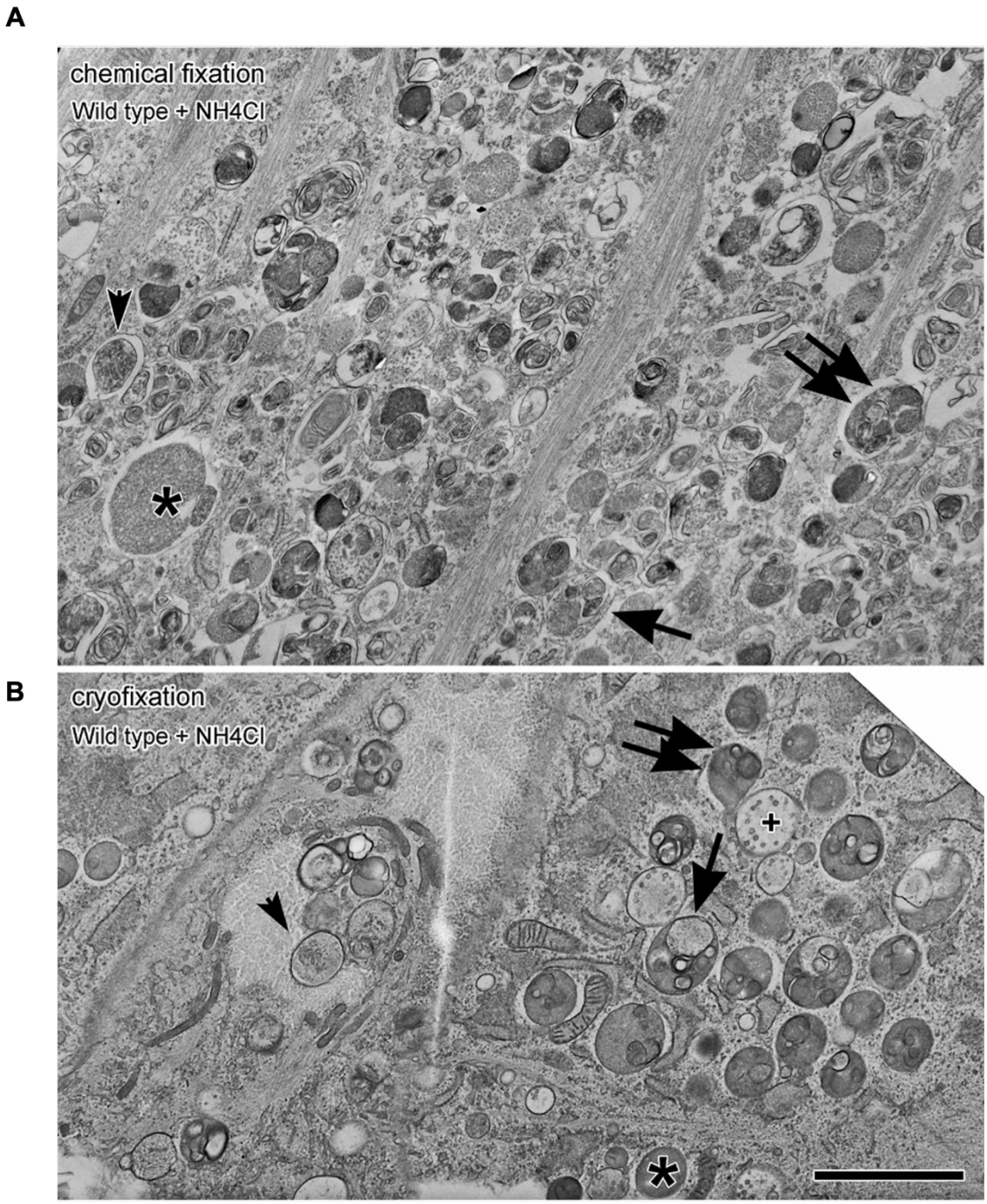

Supplementary Figure S1: Electron micrographs of wild-type fibroblasts treated with NH_4Cl comparing ultrastructure preservation achieved with conventional chemical fixation (**A**) versus rapid cryofixation (**B**). Autophagosome=arrow-head, multivesicular late endosome=cross, lysosome=asterisk, immature autolysosome=arrow, degradative autolysosome=double arrows; for explanations of organelle lettering, see Supplementary Figure S2. Scale bar=2µm.

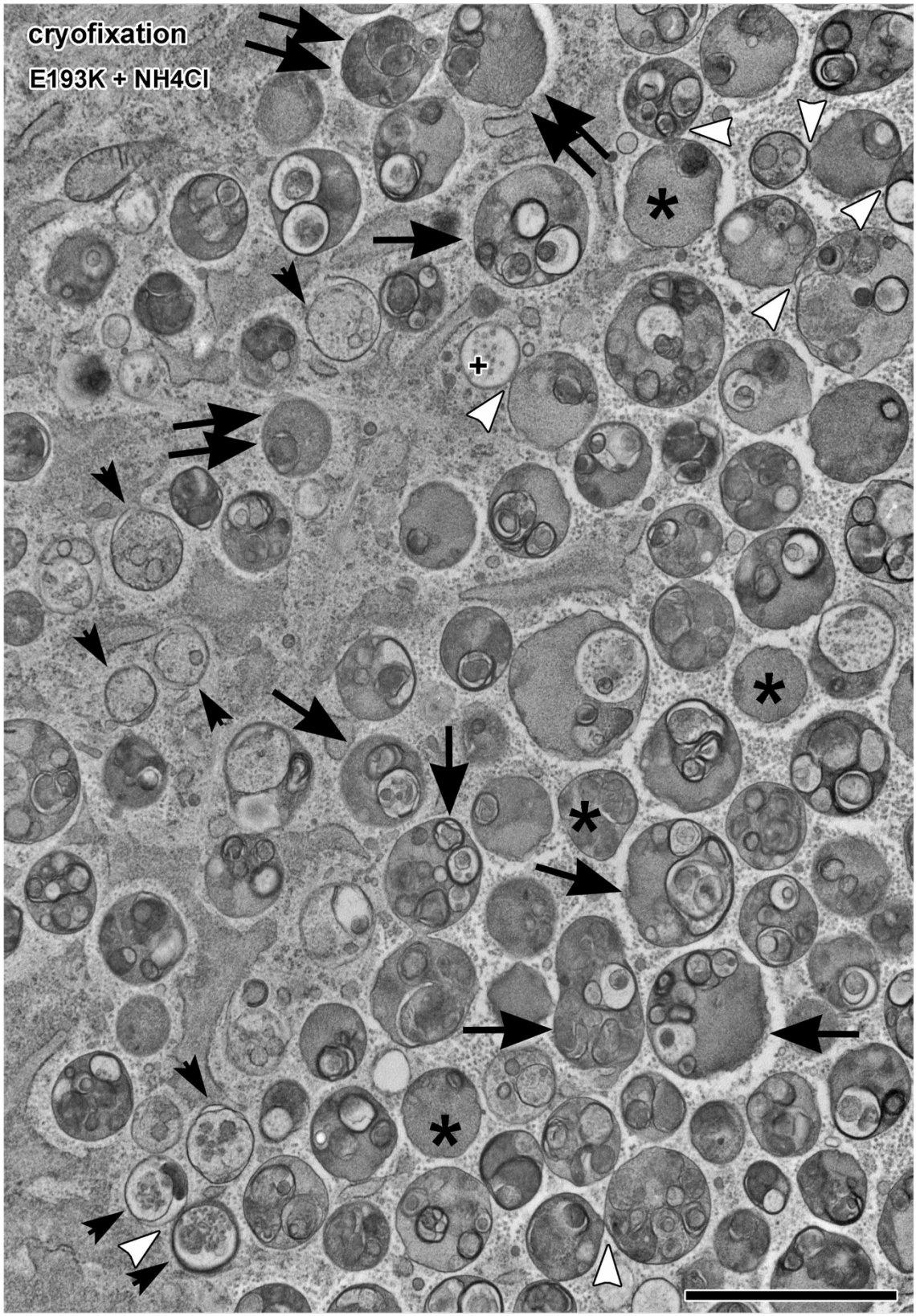

Supplementary Figure S2. Synoptic illustration of the maturation stages of autophagic organelles in E193K fibroblasts (treated with NH_4Cl) as seen by thin section transmission electron microscopy of rapidly cryo-fixed samples. The first distinct structures to be unequivocally identified as autophagic endomembranes are phagophores (i.e., disc- or cup-shaped membrane cisternae) engulfing damaged/toxic constituents, thereby transforming into autophagosomes (i.e., (organelle harboring) islets of cytoplasm

surrounded by 2 sheets of membrane bilayer: “double membrane”) – both marked here with arrowheads. Subsequently, autophagosomes meet and/or fuse with catabolic endo-lysosomal organelles (multivesicular late endosomes (marked with a cross), lysosomes (asterisks)). The resulting heterogeneous population of hybrid organelles, commonly termed autolysosomes, gets increasingly acidic and enriched in proteolytic enzymes. Putatively immature autolysosomes are marked here with arrows. Mature, degradative autolysosomes (marked with double arrows) dissolve then the previously trapped constituents, finally becoming (terminal) lysosomes (asterisks). White arrow heads mark point or surface contacts between all kinds of autophagic and endo-lysosomal organelles (homo- and heterotypic organelle fusions, regularly occurring as well, are not shown here). Visual examination for the subcellular characterization of each genotype and condition was performed on ≥100 EM-samples in total (3 independent cell culture experiments per condition). It clearly showed that the morphology of each organelle “class” did not differ between genotypes (compare, for example, Supplementary Figure S2 with S1B). Notably, autolytic organelles (pooled) were almost the same size and reacted similarly to 24h NH_4Cl exposure in E193K and control cells – a feature of this variant diverging from reports on G2019S (see Refs: [61,62]) with inflated, inefficient autolysosomes. Measuring E193K vs. WT control cells yielded the following organelle diameters in nm (± SEM): steady state: E193K: 582 ± 8.9 vs. WT 542 ± 6.6; NH_4Cl: E193K: 761 ± 11.33 vs. WT: 795 ± 14.3; ≥160 organelles/condition; n=3. Scale bar=2μm.

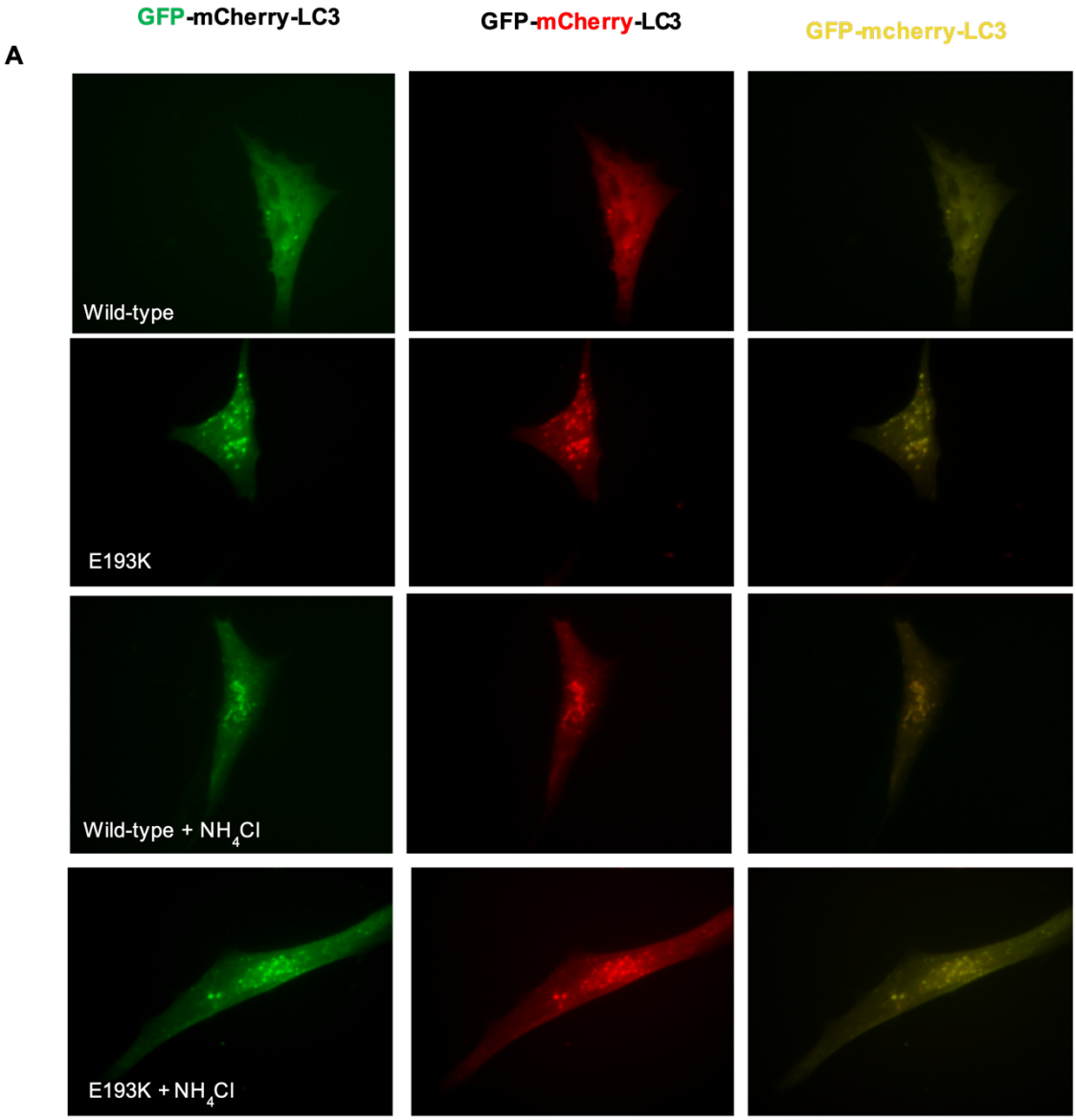
A
GFP-mCherry-LC3
GFP-mCherry-LC3
GFP-mcherry-LC3
Wild-type
E193K
Wild-type + NH4Cl
E193K + NH4Cl

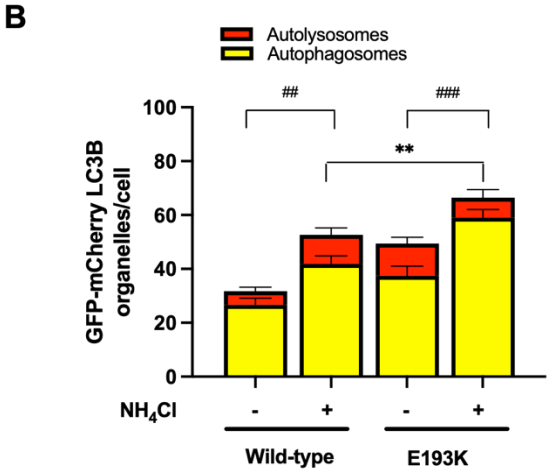
B
Autolysosomes
Autophagosomes
##
###
**
GFP-mCherry LC3B organelles/cell
100
80
60
40
20
0
NH4Cl
-
+
-
+
Wild-type
E193K

Supplementary Figure S3: Evaluation of autophagic flux by the fluorescent GFP-mCherry-LC3B reporter in wild-type and E193K human fibroblasts. Cells were transiently transfected with GFP-mCherry-LC3B for 48h and optionally treated with NH_4Cl (5mM, 24h). (**A**) Autophagosomes (non-acidic vesicles) are visualized as yellow dots, while mature, degradative autolysosomes (acidic vesicles) appear as red dots. (**B**) The graph represents the number of autophagosomes (yellow) and autolysosomes (red) for each genotype and treatment. Data are expressed as mean ± SEM, n=3 (6-8 cells for each experiment). **p<0.01; ##p<0.01, ###p<0.001. Two-Way ANOVA.

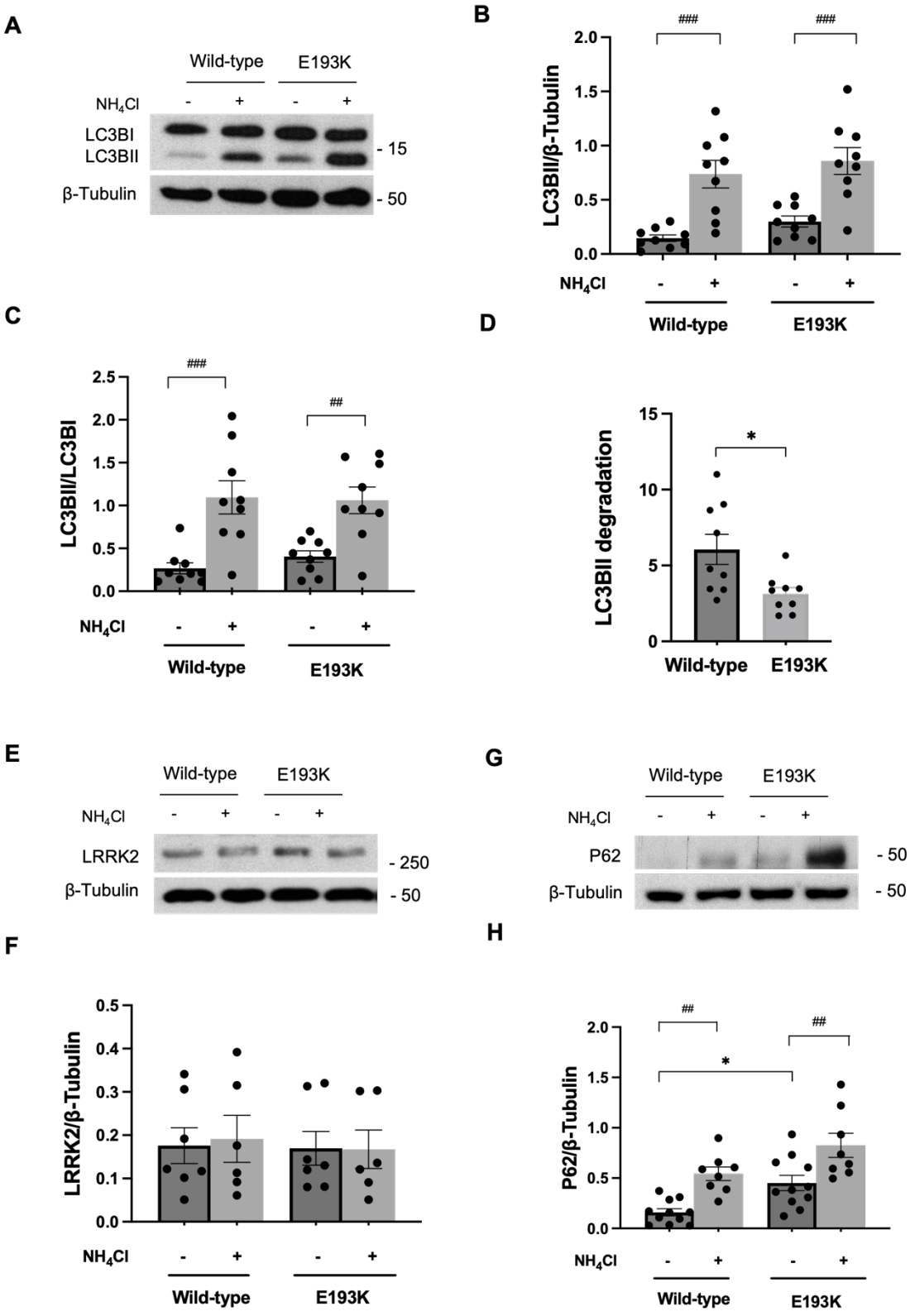

Supplementary Figure S4. LRRK2 E193K mutation affects autophagy and impairs LC3BII and P62 degradation. (**A**) LC3BII and LC3BI protein levels, (**E**) LRRK2 protein expression and (**G**) P62 protein levels in human primary fibroblasts harboring wild-type and E193K variants, treated with NH_4Cl (5 mM, 24h) when indicated, were analyzed by Western-Blot. The graphs report LC3BII (**B**), LRRK2 (**F**) and P62 (**H**) levels expressed by measuring the optical density of each band and normalized versus β-tubulin amount. (**C**) The graph shows LC3BII/LC3BI ratio by quantification of LC3BII and LCBI bands. (**D**) The graph represents LC3BII degradation. It was calculated by subtracting LC3BII band intensity between

NH_4Cl treated and untreated group normalized versus β-tubulin amount, for each genotype. Data are expressed as mean ± SEM, n=7-9 *p<0.05, ##p<0.01, ###p<0.001, Two-way ANOVA (B, C and H); *p<0.05, Student t test (D).

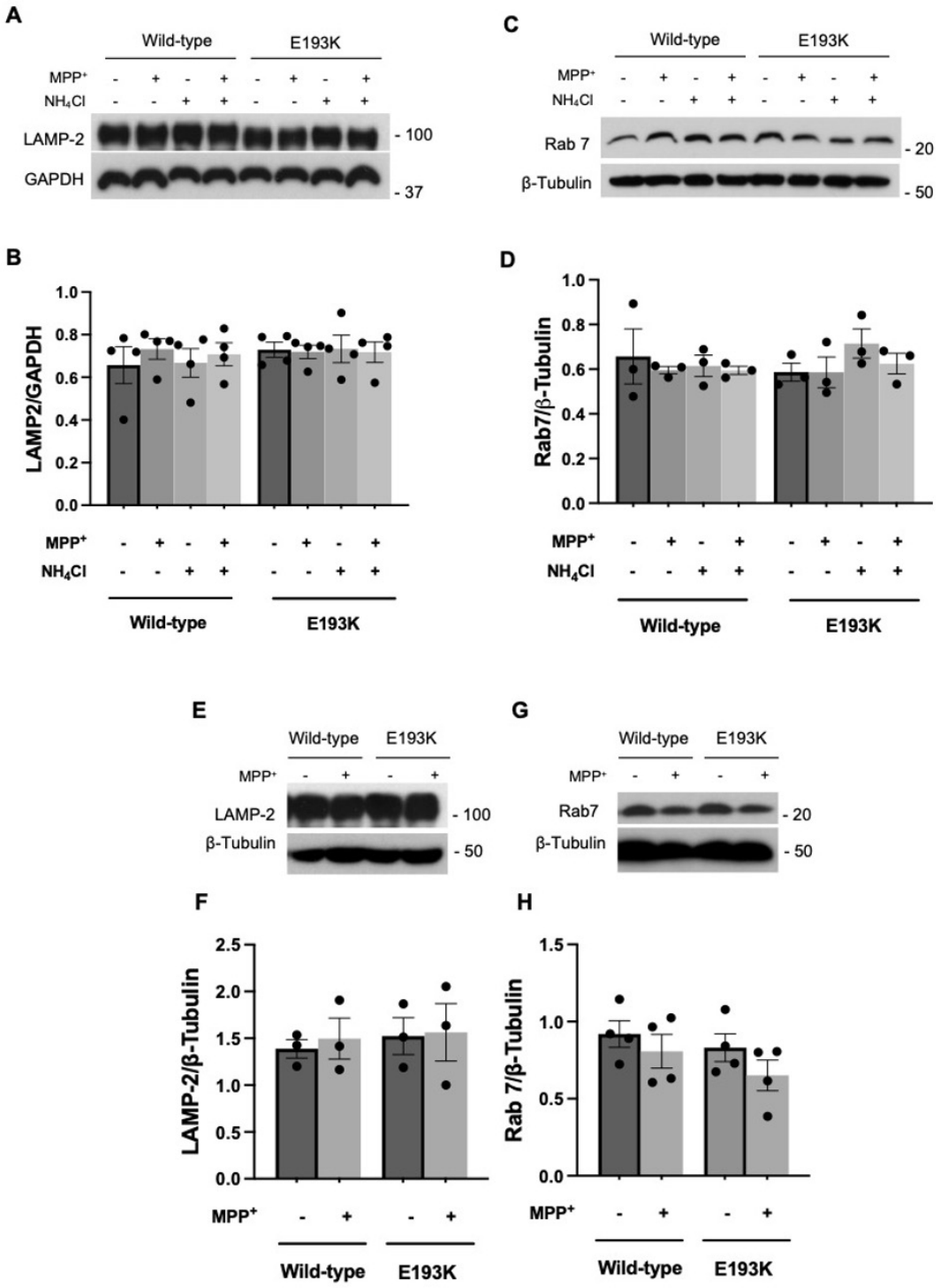

Supplementary Figure S5: Characterization of LAMP-2 (**A**) and Rab 7 (**C**) protein levels in human primary fibroblasts carrying wild-type and E193K LRRK2 mutation, treated with NH_4Cl (5mM, 24h) and/or MPP^+ (1mM, 24h) when indicated, by Western-Blot. The graphs report LAMP-2 (**B**) and Rab 7 (**D**) levels expressed by measuring the optical density of each band and normalized versus GAPDH or β-tubulin amount. LAMP-2 (**E**) and Rab 7 (**G**) protein levels in HEK 293 cells overexpressing LRRK2 wild-type and E193K LRRK2 mutation, treated with MPP^+ (1mM, 24h) were evaluated by Western-Blot. The graphs report LAMP-2 (**F**) and Rab 7 (**H**) levels expressed by measuring the optical density of each band and normalized versus β-tubulin amount. Data are expressed as mean ± SEM, n=3-4.